Cytotherapy 24 (2022) 597–607

Contents lists available at ScienceDirect

CYTOTHERAPY

journal homepage: www.isct-cytotherapy.org

FULL-LENGTH ARTICLE
Basic Research

Dental pulp stem cell-derived extracellular matrix: autologous tool boosting bone regeneration

Milda Alksne[1,*], Migle Kalvaityte[1], Egidijus Simoliunas[1], Ieva Gendviliene[2], Povilas Barasa[1], Ieva Rinkunaite[1], Algirdas Kaupinis[1], Dmitrij Seinin[3], Vygandas Rutkunas[2], Virginija Bukelskiene[1]

[1] *Institute of Biochemistry, Life Sciences Center, Vilnius University, Vilnius, Lithuania*
[2] *Institute of Odontology, Faculty of Medicine, Vilnius University, Vilnius, Lithuania*
[3] *National Center of Pathology, Affiliate of Vilnius University Hospital Santaros Klinikos, Vilnius, Lithuania*

ARTICLE INFO

Article History:
Received 9 June 2021
Accepted 5 February 2022

KeyWords:
bone
bone regeneration
dental pulp stem cell-derived extracellular matrix
dental pulp stem cells
extracellular matrix

ABSTRACT

Background aims: To facilitate artificial bone construct integration into a patient's body, scaffolds are enriched with different biologically active molecules. Among various scaffold decoration techniques, coating surfaces with cell-derived extracellular matrix (ECM) is a rapidly growing field of research. In this study, for the first time, this technology was applied using primary dental pulp stem cells (DPSCs) and tested for use in artificial bone tissue construction.
Methods: Rat DPSCs were grown on three-dimensional-printed porous polylactic acid scaffolds for 7 days. After the predetermined time, samples were decellularized, and the remaining ECM detailed proteomic analysis was performed. Further, DPSC-secreated ECM impact to mesenchymal stromal cells (MSC) behaviour as well as its role in osteoregeneration induction were analysed.
Results: It was identified that DPSC-specific ECM protein network ornamenting surface-enhanced MSC attachment, migration and proliferation and even promoted spontaneous stem cell osteogenesis. This protein network also demonstrated angiogenic properties and did not stimulate MSCs to secrete molecules associated with scaffold rejection. With regard to bone defects, DPSC-derived ECM recruited endogenous stem cells, initiating the bone self-healing process. Thus, the DPSC-secreted ECM network was able to significantly enhance artificial bone construct integration and induce successful tissue regeneration.
Conclusions: DPSC-derived ECM can be a perfect tool for decoration of various biomaterials in the context of bone tissue engineering.

Introduction

Bone tissue, in the case of various types of minor damage, can regenerate naturally. The most common example of bone regeneration is the healing of fractures [1]. However, there are many clinical cases where fractures do not heal independently (e.g., 13% of all tibial fractures) [2]. Moreover, there are many other clinical situations where bone tissue damage (caused by genetic diseases, cancer, various types of inflammation, etc.) results in critical-size bone defects that are also unable to regenerate naturally [2,3]. In an attempt to regenerate damaged bone tissue, orthopedic transplant surgeries are performed. To date, autologous transplants have been considered the gold standard for this kind of surgery [4]. However, these transplants have disadvantages, including limited donor tissue sources and donor site morbidity [5–7]. To address this issue, scientists around the globe are actively working to create fully functional artificial bone that can be used for treatment of critical-size bone defects.

Although many different production technologies are being developed and tested to reach this goal, all researchers agree on three main elements that should be combined: cells, scaffolds and bioactive molecules [8]. Bioactive molecules are usually used for scaffold surface decoration. Decorated scaffolds not only integrate more easily into the patient's body but also promote faster regeneration of damaged bone and even accelerate angiogenesis [5]. Three main types of bioactive molecules used for bone scaffold enrichment can be distinguished: (i) growth factors (e.g., bone morphogenetic protein 2, bone morphogenetic protein 7, platelet-derived growth factor, vascular endothelial

* Correspondence: Milda Alksne, PhD, Institute of Biochemistry, Life Sciences Center, Vilnius University, Sauletekio Ave. 7, Vilnius LT-10257, Lithuania.
E-mail address: milda.peciukaityte@gf.vu.lt (M. Alksne).

https://doi.org/10.1016/j.jcyt.2022.02.002
1465-3249/

growth factor) [9–11], (ii) various extracellular matrix (ECM) proteins and their signaling sequences (e.g., RGD, B2A2-K-NS and P-15 peptides, collagen, fibronectin) [12–16] and (iii) small signaling molecules (e.g., quercetin, silibinin, hesperetin, icariin) [17–20]. However, using molecules/proteins of only one type fails to significantly improve the osteoinductive properties of the scaffold [21].

Recently, a new and relatively simple surface decoration method has been gaining more and more attention: coating the scaffold with cell culture-derived ECM. Compared with single proteins or signaling molecules, natural ECM secreted by the cells has a multi-component structure, with various cell-activating ligands. These ligands initiate a cellular response that significantly improves the osteointegration process [22,23].

Despite the rapid growth of this research field, there are still a lot of uncertainties. Thus far, detailed ECM composition studies have been limited to only primary bone marrow-derived mesenchymal stem cells (BMSCs), adipose stromal cells (ASCs), dermal fibroblasts, osteoblast/fibroblast co-cultures and ECM formed by osteoblast cell lines [22,24–29]. Based on these studies, the matrisome (all ECM proteins produced by one organism or cell/tissue type [30]) signature of osteogenic ECM differs depending on the cell type used for production. Some similar core matrisome components (e.g., collagen 2, collagen 5, fibronectin) have been detected in all analyzed ECMs. However, the majority of the determined proteins have been cell type-specific (e.g., lysyl oxidase homolog 2 [LOXL2] and collagen 8 proteins were detected in BMSC ECM but not in matrix formed by dermal fibroblasts) [27,28]. These different ECM proteins, in turn, can trigger different signaling cascades within the cells [30]. Therefore, to apply this scaffold decoration method in practice, it is necessary to analyze in detail the different types of ECMs as well as the potential cellular response induced by them.

Furthermore, to use cell-derived, ECM-coated scaffolds to treat damaged bone, they must be easily applicable in a clinical setting. However, the extraction procedure for cells forming the aforementioned ECMs is complicated and painful and requires additional surgical interventions to the patient's body [31,32]. Moreover, BMSCs, ASCs and fibroblasts are able to form bone-specific ECM networks only after additional stimulation with chemical inductors (e.g., β-glycerophosphate, dexamethasone) [33], which may adversely affect the patient's body. Thus, attempts are being made to proceed to clinical trials using adult stem cells that can spontaneously differentiate into the osteogenic lineage and be extracted without aggressive surgical interventions. One possible candidate could be dental pulp stem cells (DPSCs) [34,35]. However, thus far, no studies have been conducted in which ECM formed by DPSCs has been tested.

This study was carried out to evaluate the impact of DPSC-secreted ECM on new bone formation. ECM-coated surfaces were prepared by culturing laboratory rat DPSCs on three-dimensional (3D)-printed porous polylactic acid (PLA) scaffolds. The structure and matrisome composition of the DPSC-derived ECM were characterized comprehensively. The effect of ECM on newly seeded DPSC adhesion, migration, proliferation and osteogenic differentiation was investigated. Moreover, the angioinductive and immunogenic properties of the ECM were elucidated. Finally, PLA scaffolds coated with DPSC-ECM were implanted into critical-size rat calvarial defects to assess the ability of DPSC-ECM to promote bone regeneration *in vivo*.

Methods

Scaffold 3D printing

PLA pellets (racemic L/D isoform polymer, particle size 100–800 μm, molecular weight 42 700 g/mol) (STP Chem Solutions Co Ltd, Nonthaburi, Thailand) were used for scaffold production. PLA filament preparation and scaffold models as well as their 3D printing procedures were performed as described by Alksne *et al.* [36]. The 3D-printed eight-layered woodpile scaffolds (30 × 30 × 1.6 mm) (Figure 1A) were further cut into 10 × 10 × 1.6-mm pieces for *in vitro* studies and into 5.5-mm-diameter circles for *in vivo* experiments.

Preparation and maintenance of primary cell culture

Wistar rat-derived DPSCs and pulmonary trunk blood vessel endothelial stem cells (PTEC) were used for *in vitro* studies. In all experiments, the use of rats as well as their DPSCs and PTECs was approved by the Vilnius animal research ethics committee, Lithuania (G2-40; March 18, 2016). Cell isolation and characterization protocols are described in the supplementary material. Isolated DPSCs and endothelial stem cells were maintained in growth medium (GM); Iscove's Modified Dulbecco's Medium (Gibco, Carlsbad, CA, USA) supplemented with 10% fetal bovine serum (Gibco) and antibiotic solution composed of penicillin 100 U/mL and streptomycin 100 mg/mL (Gibco) at 37°C in a humidified atmosphere containing 5% carbon dioxide. The cells used in the experiments were cultivated up to 20 passages.

Decellularized scaffold production

To produce PLA scaffolds coated with cell-derived ECM, DPSC suspensions (3×10^4 cells/cm^2) were seeded on pure PLA scaffolds. Cell–scaffold constructs were cultivated for 7 days in GM containing 100 μg/mL ascorbic acid solution composed of 5 mg/mL L-ascorbic acid 2-phosphate (Sigma-Aldrich, St Louis, MO, USA) diluted in phosphate-buffered saline (PBS) (Gibco), and half of the medium was changed every second or third day. After 7 days, scaffolds were washed twice with PBS and transferred to a −20°C freezer for 30 min. Decellularization solution composed of 0.5% Triton X-100 (AppliChem GmbH, Darmstadt, Germany) and 20 mM ammonium hydroxide (Sigma-Aldrich) prepared in PBS was added to the samples and incubated for 1 h with gentle shaking at 25 rpm using a WT17 (Biometra GmbH, Göttingen, Germany) at 37°C. Later, decellularization solution was aspirated, specimens were rinsed twice with PBS and nuclease solution composed of 10 U/mL DNase I (Thermo Fisher Scientific, Waltham, MA, USA), 100 μg/mL RNase A (Thermo Fisher Scientific) and 10 mM magnesium chloride (Sigma-Aldrich) prepared in PBS was added and incubated for 1 h with gentle shaking at 25 rpm at 37°C. After the predetermined time, the nuclease solution was aspirated and samples were washed twice with PBS. In addition, 0.1% glutaraldehyde (Sigma-Aldrich) solution prepared in PBS was added and incubated for 4–6 h at 4°C. Next, specimens were rinsed with PBS and immersed in 0.1 M glycine (Invitrogen, Carlsbad, CA, USA) solution prepared in PBS and incubated overnight at 4°C. The next day, samples were again washed twice with PBS and stored in PBS at 4°C until use.

Sample for liquid chromatography–mass spectrometry preparation

To extract the proteins retained on the scaffolds after the decellularization procedure, samples were treated with lysis buffer composed of 8 M urea (Sigma-Aldrich), 2% 3-[(3-cholamidopropyl) dimethylammonio]-1-propanesulfonate hydrate (Sigma-Aldrich), 4% sodium dodecyl sulfate (Sigma-Aldrich) and 100 mM dithiothreitol (Thermo Fisher Scientific) in deionized water for 10 min. Next, the supernatants were collected and trypsin digestion was performed according to the filter-aided sample preparation protocol described by Wiśniewski *et al.* [37].

Liquid chromatography–mass spectrometry-based protein identification

Liquid chromatography analysis was performed using an Acquity ultra-performance liquid chromatography system (Waters Corporation, Wilmslow, UK). Peptide separation was performed on an Acquity ultra-performance liquid chromatography HSS T3 250-mm analytical column. Data were acquired using a Synapt G2 mass

spectrometer with MassLynx 4.1 software (Waters Corporation) in positive ion mode using data-independent acquisition (ultra-definition MS^E). Raw data were locked mass-corrected using the doubly charged ion of [Glu1]-fibrinopeptide B (m/z 785.8426; [M+2H]2+). Raw data files were processed and searched using ProteinLynx Global SERVER 3.0.1 (Waters Corporation). Data were analyzed using trypsin as the cleavage protease, and one missed cleavage was allowed. Fixed modification was set to carbamidomethylation of cysteines, and variable modification was set to oxidation of methionine. Minimum identification criteria included one fragment ion per peptide and three fragment ions and one peptide per protein. The following parameters were used to generate peak lists: (i) low energy threshold was set to 150 counts, (ii) elevated energy threshold was set to 50 counts and (iii) intensity threshold was set to 750 counts. UniProtKB/Swiss-Prot rat and bovine databases (September 24, 2020) were used for protein identification. The UniProtKB database (December 6, 2020) was used to classify proteins with respect to their cellular components. Extracellular region proteins were grouped into six categories of ECM proteins according to the Matrisome Project [38]. The Enrichr analysis tool (December 29, 2020) was used for Gene Ontology (GO) mapping and functional annotation of proteins.

Spontaneous osteogenic differentiation

DPSCs were grown on tested scaffolds for 1 day, 7 days and 10 days. The numbers of seeded cells are listed in supplementary Table 1. Samples were maintained in GM at 37°C in a humidified atmosphere containing 5% carbon dioxide, and half of the GM was changed every 2–3 days.

Alkaline phosphatase assay

Alkaline phosphatase (ALP) activity was evaluated using the Phosphatase Substrate Kit (Thermo Fisher Scientific). Assay was performed according to the manufacturer's protocol. Results were normalized according to cell numbers determined on each type of scaffold (seeded identically) after each time point. Cell numbers on scaffolds were determined by 4′,6-diamidino-2-phenylindole assay [39].

Determination of collagen amount

The amount of collagen was determined by the Sirius Red assay. All procedures were performed as described by Alksne *et al.* [36]. Scaffolds without cells were used to assess background value.

ECM mineralization assay

ECM mineralization during spontaneous DPSC osteogenesis was evaluated by Alizarin Red S assay. All procedures were performed as described by Alksne *et al.* [40]. Scaffolds without cells were used to evaluate the background value.

Quantitative polymerase chain reaction

Runx2 and osteopontin (OPN) protein messenger RNA (mRNA) expression levels in differentiated DPSCs were evaluated by quantitative polymerase chain reaction (qPCR). Cell lysis, RNA extraction, complementary DNA synthesis and gene quantification procedures were performed as described by Alksne *et al.* [40]. Obtained gene expression levels were calculated using $2^{-\Delta\Delta Ct}$ method [41]. Results were normalized according to the expression of glyceraldehyde 3-phosphate dehydrogenase and standardized according to undifferentiated cells seeded on a standard tissue culture plate surface at an initial time point. Primer pair sequences used for qPCR assay are listed in supplementary Table 2.

Cytokine evaluation in DPSC secretome

To evaluate cytokines that were secreted by DPSCs cultivated on tested scaffolds, cells (1×10^3 cells/cm^2) were grown on scaffolds for 7 days. Scaffolds were then rinsed twice with PBS and transferred to new plate wells containing GM without fetal bovine serum. After 48 h, GM was collected and centrifuged for 4 min at 1000 g (HERMLE Labortechnik GmbH, Wehingen, Germany). Supernatants were transferred to new tubes and stored at −20°C until use. Dot blot analysis of cytokines presented in collected secretomes was performed using the Rat Cytokine Array Kit (R&D Systems, Minneapolis, MN, USA). All procedures were performed according to the manufacturer protocol.

Bone regeneration evaluation in critical-size Wistar rat calvarial defect model

Two groups of scaffolds, PLA and PLA+ECM, were evaluated for bone regeneration in the critical-size Wistar rat calvarial defect model. Procedures were performed at the Department of Biological Models, Institute of Biochemistry, Life Sciences Center, Vilnius University (Vilnius, Lithuania). The sample size was determined with G*Power 3.1.9.7 software [42] using the difference between two independent means test with a priori analysis (α = 0.05, power = 0.8, f effect size = 1.7). Four female and four male 4-month-old Wistar rats (approximate weight 300 g) were used for scaffold implantation.

The animals were anesthetized with an intraperitoneal injection of 2% Xylazine 5 mg/kg (Alfasan International B.V., Woerden, the Netherlands) and 100 mg/mL ketamine hydrochloride at 2.4 mL/kg (Rotexmedica GmbH, Trittau, Germany). Surgical procedures were performed as described by Gendviliene *et al.* [43]. Afterward, the rats were transferred to individual enriched cages and observed for 8 weeks. The first dose (0.01 mg/kg) of 0.3 mg/mL buprenorphine hydrochloride (Richter Pharma AG, Wels, Austria) was given subcutaneously 3 h after the surgery and then according to need up to two times per day for 3 days. The rats were kept in a controlled environment at 22 ± 1°C with humidity of 55 ± 3% and a 12/12-h light–dark cycle and received a standardized diet and water ad lib. After 8 weeks, rats were euthanized using carbon dioxide overdose, and specimens were harvested and fixed in 10% (v/v) neutral buffered formalin.

Micro-computed tomography

The specimens were scanned with an x-ray 3D computed tomography (CT) device (250E; RayScan Technologies GmbH, Meersburg, Germany). Scanning and bone volume (mm^3) calculation procedures were performed as described in a previous study [43].

Histology

Sample histology evaluation was done to count the newly formed bone area (mm^2). Specimen decalcification, staining and qualitative and quantitative procedures were performed as described in a previous study [43]. Additional details regarding the methods used in this study are provided in the supplementary material.

Statistical analysis

Statistical analysis was conducted using RStudio v1.1.442. The qPCR results were additionally analyzed with Rotor-Gene 6000 Series Software 1.7. The data are presented as median ± interquartile range of three independent experiments (n ≥3 samples per group). Focal adhesion results are presented with a distribution density function. Shapiro–Wilk test was used to evaluate data normality (when n ≥5). Kruskal–Wallis one-way analysis of variance and post-hoc Tukey tests were used to determine the significant differences of not

normally distributed data between three or more groups. One-way analysis of variance and post-hoc Tukey tests were used to evaluate normally distributed results (when n ≤ 5) between three or more groups. Statistical significance was determined to be $P \leq 0.05$.

Results

Cell characterization

DPSCs were isolated from the dental pulp of rat incisors. Flow cytometry analysis of surface markers showed that these cells were positive for mesenchymal stromal cells (MSC)-specific surface antigens CD44, CD54 and CD90 and negative for hematopoietic and endothelial markers CD13, CD14 and CD31 (see supplementary Figure 1).

PESCs were isolated from rat vascular trunks. Surface antigen analysis by flow cytometry demonstrated that these cells were positive for CD54 and CD90 and negative for markers CD13, CD14, CD44 and CD45 (see supplementary Figure 2A). Additionally, by using immunocytochemistry assay, the authors showed that isolated PESCs expressed another endothelial cell marker—CD31—on their surface (see supplementary Figure 2B). Finally, two other endothelial cell properties were confirmed: isolated PESCs were capable of forming vessel-like structures on Matrigel (Sigma-Aldrich) (see supplementary Figure 2C) and were able to uptake modified acetylated low-density lipoprotein (see supplementary Figure 2D).

DPSC-secreted ECM characterization

First, the authors evaluated the efficiency of the scaffold decellularization process. This was assessed qualitatively by visualizing cell cytoskeletal protein actin and ECM protein fibronectin retention on scaffolds and quantitatively by measuring the amount of DNA traces remaining after the cell removal procedure (Figure 1B,C). Cell-free PLA scaffolds were used as a control.

The qualitative assessment showed that the cell removal technique used by the authors was effective (Figure 1B). Intact DPSC-formed ECM was maintained during the procedure, as evidenced by the fibronectin network remaining on the scaffolds. Moreover, cellular cytoskeletal proteins were removed, and no actin network remained on the scaffolds after the procedure. These results were also confirmed by quantitative evaluation of the amount of DNA on the samples (Figure 1C). It should be noted that the amount of DNA on the PLA+ECM scaffolds corresponded to that found on the control surface.

The detailed composition of proteins retained on PLA scaffolds was characterized by proteomic analysis. A total of 403 proteins were detected. These proteins were found in membrane (47), cytoplasm (142), organelle (42), nucleus (53), cytoskeleton (67) and extracellular region (52) (Figure 1D). Thus, the authors observed that it was not only ECM proteins that remained on the scaffolds after the decellularization procedure. Although the number of extracellular region proteins was less than 20%, more than 70% of these were assigned as core matrisome (16) or matrisome-associated (22) proteins. In addition to matrisome proteins, DPSC-formed ECM contained regulators, secreted factors and other ECM-affiliated proteins (14) (Figure 1E). The complete list of detected proteins is presented in supplementary Table 3. GO analysis of proteins belonging to the extracellular region suggested that DPSC-formed ECM contributes to biological processes associated with bone/cartilage formation, angiogenesis, ECM formation, immune response, protein processing and membrane transport (Figure 1F). A detailed list of determined biological processes is laid out in supplementary Table 4.

ECM effect on DPSC behavior

The authors evaluated the impact of DPSC-formed ECM on cell adhesion, motility and proliferation efficiency. For the evaluation of cell adhesion, DPSCs were seeded on PLA or PLA+ECM scaffolds, and cell surface area was analyzed 0.5 h, 2 h and 24 h post-seeding by visualizing the F-actin filaments. Fluorescence microscopy images of F-actin filaments (see supplementary Figure 3) and cell surface area measurements (Figure 2B) showed that after all analyzed time intervals, cells attached better to ECM-coated scaffolds. Correspondingly larger DPSC surface area was also demonstrated compared with pure PLA scaffolds ($P < 0.001$).

To better understand the influence of DPSC-formed ECM on the cell attachment process, focal adhesions formed within DPSCs 24 h post-seeding were qualitatively and quantitatively evaluated (Figure 2A,C). The results indicated that compared with pure PLA samples, the PLA+ECM surface demonstrated a higher number of focal adhesions within the cells (i.e., ECM-coated scaffolds were more attractive for DPSC attachment) ($P < 0.001$).

To evaluate the influence of DPSC-formed ECM on cell motility, scaffolds were incubated on a monolayer of DPSCs for 72 h and the number of cells that migrated onto these specimens was then determined (Figure 2D). The results showed that the ECM-coated surface was more attractive for DPSC migration, with a higher cell count being demonstrated on PLA+ECM scaffolds compared with pure PLA samples ($P < 0.05$).

Assessment of cell proliferation activity indicated that cell numbers registered at 24 h, 48 h and 72 h post-seeding were almost the same on both scaffolds (PLA and PLA+ECM), with DPSCs proliferating equally well on both groups of specimens (Figure 2E). However, differences between the PLA and PLA+ECM groups appeared later, at 96 h and 120 h post-seeding. During these time intervals, DPSCs showed significantly better proliferative activity on PLA+ECM scaffolds compared with PLA scaffolds.

ECM impact on DPSC osteogenic differentiation in vitro

To determine the cell-derived ECM effect on the induction of osteogenic differentiation in DPSCs, ALP activity, osteogenic-related gene expression and bone tissue-specific ECM were analyzed. Runx2 and OPN protein mRNA expression analysis showed that both tested scaffolds stimulated DPSC differentiation toward an osteogenic lineage via upregulation of protein Runx2 and OPN mRNA expression (Figure 3A–E). Moreover, the highest protein Runx2 mRNA expression was determined in cells maintained on both tested scaffolds at the 10th day of differentiation (Figure 3A). However, after the first day of differentiation, protein-coding gene expression level in DPSCs grown on PLA+ECM already showed a greater increase compared with that observed in cells grown on pure PLA ($P < 0.05$). OPN protein mRNA levels remained almost unchanged on evaluation at the first and seventh days of differentiation (Figure 3B), with the highest level of expression being observed at only the 10th day of differentiation in cells grown on both investigated scaffolds. However, the authors did not detect a statistically significant difference in OPN protein mRNA expression induction in DPSCs cultivated on PLA and PLA +ECM scaffolds.

The authors found that after the first and seventh days of differentiation, PLA and PLA+ECM scaffolds did not cause differences in ALP activity within the cells (Figure 3C). The highest ALP activity in cells maintained on PLA and PLA+ECM scaffolds was detected after 10 days of differentiation. However, stronger ALP activity was registered in DPSCs grown on ECM-coated scaffolds compared with pure PLA samples ($P < 0.05$).

Bone tissue-specific ECM formation results showed that DPSCs grown on both surfaces tended to accumulate collagen in their ECM; however, the authors did not observe significant differences in the

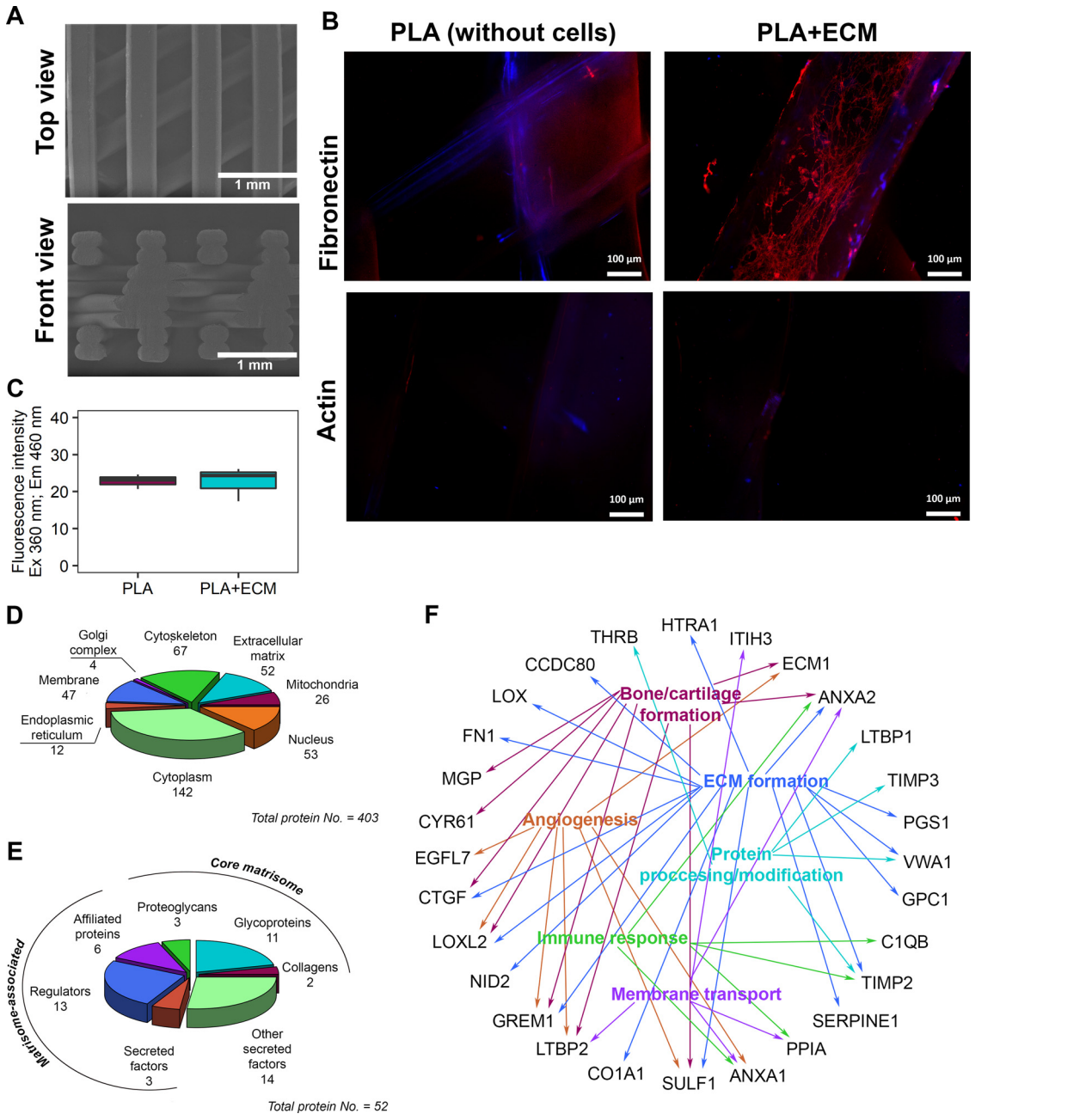

Figure 1. PLA scaffold characteristics, decellularization process effectiveness and detailed DPSC-produced ECM analysis. (A) SEM images of the 3D-printed porous PLA scaffolds. (B) Visualized fibronectin or actin filaments (red = Alexa Fluor 594) and DNA residues (blue = DAPI). (C) DNA residue quantification after cell removal procedure by DAPI assay. Results are presented as median ± IQR. (D) Proteins grouped by their cellular localization. Results are presented as a pie chart. (E) Matrisome signature of DPSC-secreted ECM. Results are presented as a pie chart. (F) Biological processes evaluated by GO analysis. DAPI, 4′,6-diamidino-2-phenylindole; IQR, interquartile range; SEM, scanning electron microscope. (Color version of figure is available online.)

impact of PLA versus PLA+ECM scaffolds on collagen accumulation (Figure 3D). By contrast, ECM mineralization results indicated that after 7 days and 10 days of DPSC cultivation on scaffolds, the greatest and most statistically significant increase in ECM mineralization was registered in cell cultures maintained on PLA+ECM specimens compared with pure PLA samples ($P < 0.001$ and $P < 0.05$, respectively) (Figure 3E).

ECM influence on the osteointegration process in vitro

The impact of DPSC-formed ECM on successful scaffold integration into tissue was investigated by imitating the scaffold implantation process *in vitro* and thus evaluating its angiogenic properties as well as the possible response of the organism (Figure 3F,G). DPSCs, which mimic the adult stem cells that migrate to the site of injury after scaffold implantation, were grown on PLA and PLA+ECM samples for 7 days. After a predetermined time, secretomes were collected from the specimens and the presence of 29 molecules was analyzed by dot blot (see supplementary Figure 4). In the secretomes from both samples, the authors observed expression of the same 11 cytokines, chemokines and growth factors: cytokine-induced neutrophil chemoattractant (CINC) 1, CINC-2α/β and CINC-3; chemokine (C-X-C motif) ligand 1; IL-1ra; IL-6; soluble intercellular adhesion molecule 1; chemokine (C-X-C motif) ligand 10; chemokine (C-C motif) ligand 5; TIMP metallopeptidase inhibitor 1; and VEGF (Figure 3G). However, the authors did not observe significant differences between scaffold impacts on the levels of detected signaling molecules.

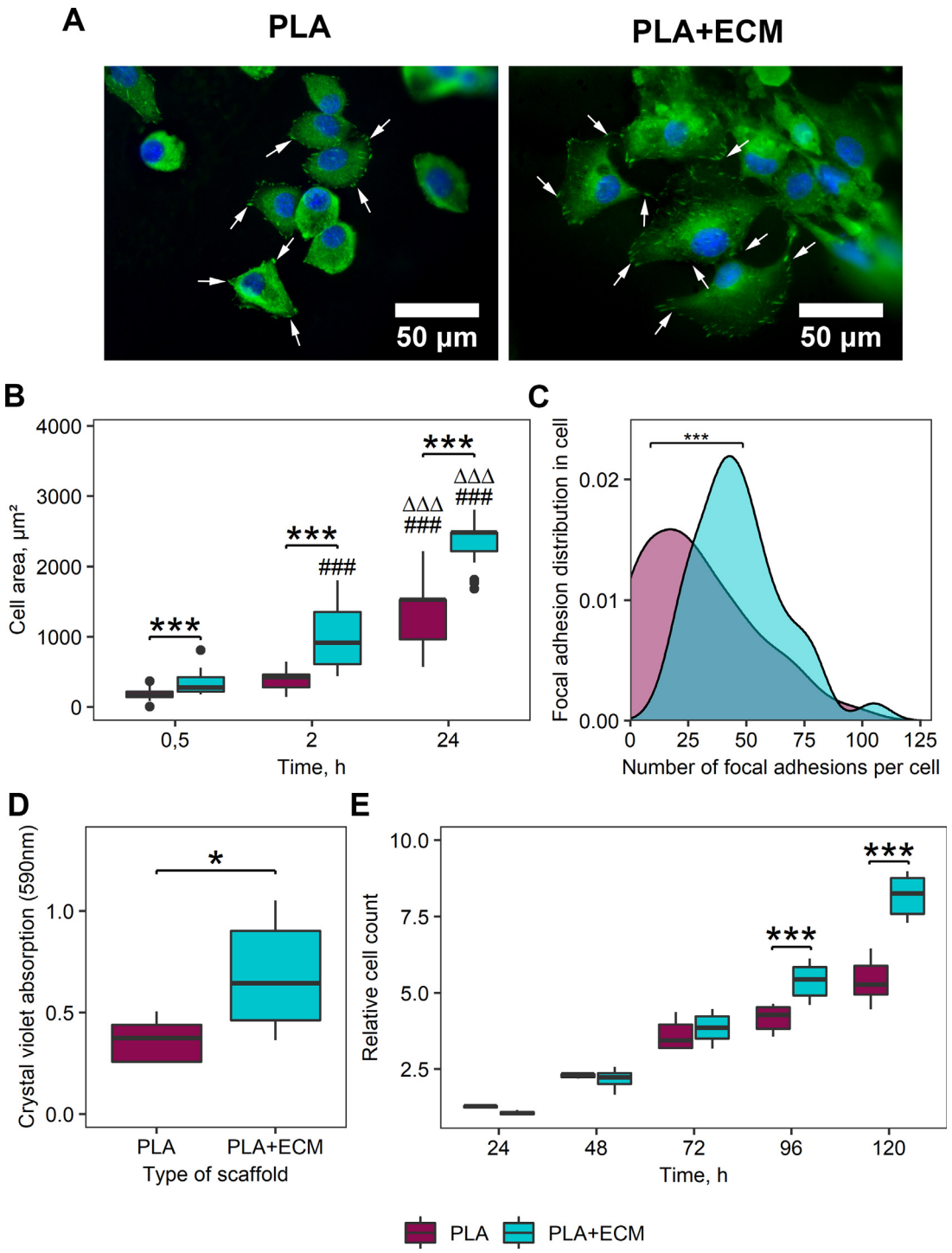

Figure 2. DPSC behavior on ECM-coated scaffolds. (A) Representative images of visualized nucleus (blue = DAPI) and FA (green = vinculin) in DPSCs. (B) Cell surface area measurement. (C) Quantification of FA spots within the cells. (D) DPSC migration onto the PLA and PLA+ECM scaffolds. (E) Cell proliferation rate. Results are standardized according to the number of cells maintained on appropriate scaffolds for 24 h. $^{*}P < 0.05$ and $^{***}P < 0.001$ (indicate significant differences between tested groups). $\#\#\#P < 0.001$ (indicates significant differences compared with 0.5 h within the same scaffold group). $\Delta\Delta\Delta P < 0.001$ (indicates significant differences in data compared with 2 h within the same group). DAPI, 4′,6-diamidino-2-phenylindole; FA, focal adhesion. (Color version of figure is available online.)

In addition, it was noted that DPSCs, which grew on both tested scaffolds (PLA and PLA+ECM), most actively synthesized the growth factor VEGF (Figure 3G). The angiogenic properties of DPSC-formed ECM were also assessed by vertical migration test of PESCs. PLA and PLA+ECM specimens were incubated on a monolayer of PESCs for 72 h, and the number of cells that migrated onto these specimens was then determined (Figure 3F). Results showed that the most attractive samples for PESC migration were PLA+ECM scaffolds, on which the highest number of cells was registered ($P < 0.001$).

ECM impact on new bone formation in vivo

The impact of DPSC-formed ECM on critical bone defect regeneration *in vivo* was assessed by micro-CT and histological evaluation.

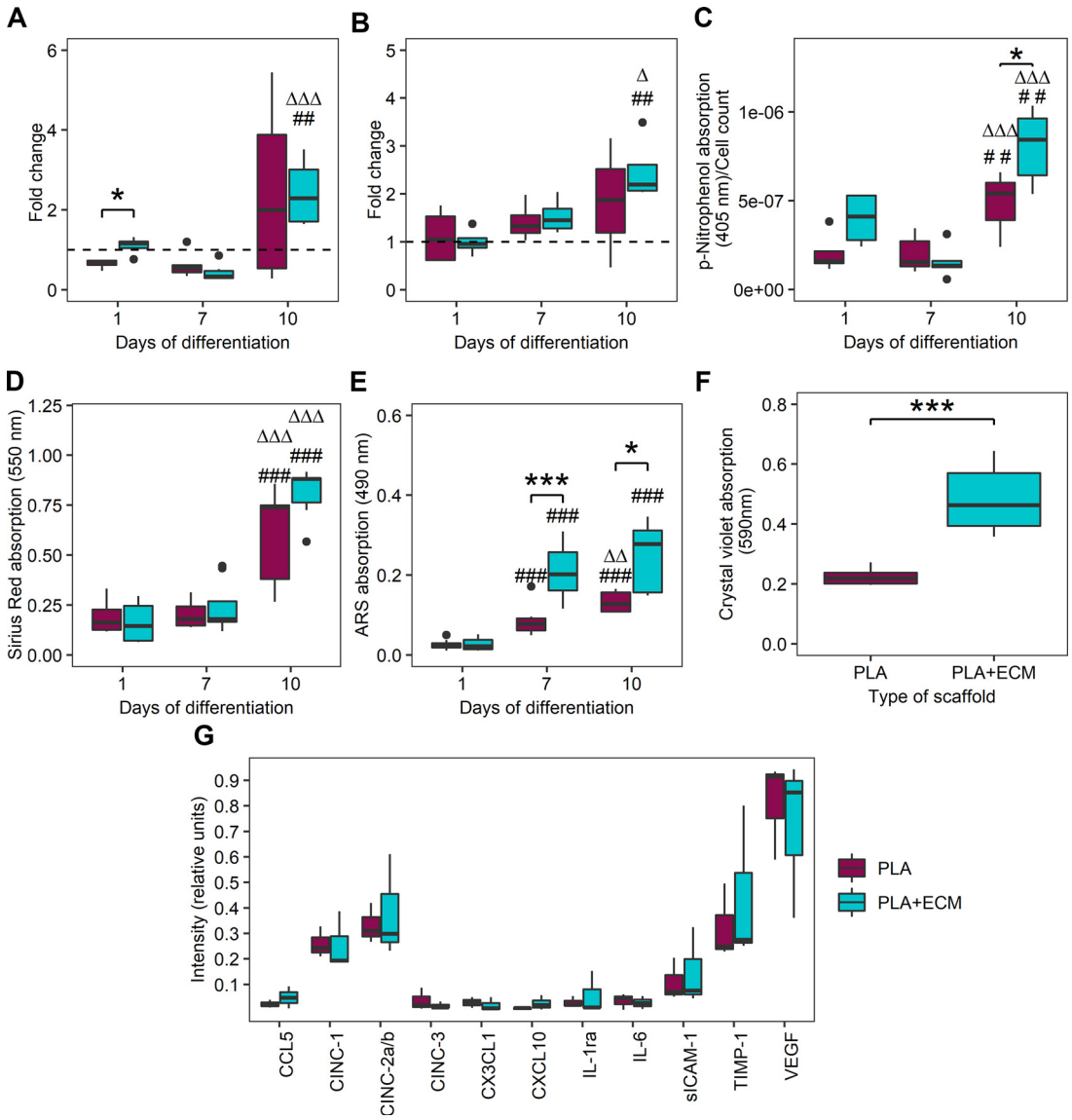

Figure 3. Impact of ECM-coated scaffold on the osteogenesis and osteointegration of DPSCs *in vitro*. (A) Runx2 protein mRNA expression level in DPSCs. (B) OPN protein mRNA expression level in DPSCs. (C) ALP activity evaluation. (D) DPSC collagen production quantification. (E) ECM mineralization analysis. (F) PESC migration onto the PLA and PLA+ECM scaffolds. (G) Dot blot analysis data of bioactive molecules detected in secretomes of DPSCs grown on tested samples. $^{*}P < 0.05$ and $^{***}P < 0.001$ (indicate significant differences between tested groups). $\#\#P < 0.01$ and $\#\#\#P < 0.001$ (indicate significant differences compared with day 1 within the same scaffold group). $\Delta P < 0.05$, $\Delta\Delta P < 0.01$ and $\Delta\Delta\Delta P < 0.001$ (indicate significant differences compared with day 7 within the same group). (Color version of figure is available online.)

The increase in new bone volume after analysis with the algorithm is shown in Figure 4.

Micro-CT evaluation of new bone formation showed no significant sex-specific differences in the PLA and PLA+ECM groups (males, $P = 0.09$, females, $P = 0.18$) (see supplementary Figure 5A). However, micro-CT results revealed a statistically significant difference between the PLA (1.9 ± 0.44 mm^3) and PLA+ECM (3 ± 0.4 mm^3) groups ($P < 0.05$) when males and females were counted together (Figure 4B).

The histological section images of different tested groups are presented in Figure 4C. These results showed that the connective tissue thickness varied from 1.0 mm to 2.0 mm in both groups, and the new bone formed a layer ranging from 0.3 mm to 1.0 mm, growing from the defect sides toward the center. Some sections of PLA+ECM scaffolds showed that new bone islands formed separately from the newly formed bone at the defect edges. Quantitative histological evaluation showed no significant sex-specific differences in new bone formation in both groups ($P > 0.05$) (see supplementary Figure 5B). However, a statistically significant difference was found between the PLA and PLA+ECM groups in males ($P < 0.005$) and females ($P < 0.05$) both separately (see supplementary Figure 5B) and together ($P < 0.0005$) (Figure 4D). Moreover, cell infiltrates were observed in both groups, indicating ongoing scaffold degradation and bone regeneration.

Discussion

It is well known that each tissue has a specific ECM composition that is required for specialized tissue homeostasis [22]. ECM is composed of two major constituents: structural components (core matrisome) and the proteins interacting with them (matrisome-associated proteins). ECM contains all instructions regarding the structure, mechanical properties and function of a tissue [44]. In case of various injuries, stem cells from adjacent tissues use this information to restore damaged sites. Various studies have shown that decellularized, tissue-specific bioinks promote cell differentiation commitment, demonstrating the possibility of adapting this technique for tissue regeneration applications [45–47]. Nevertheless, harsh

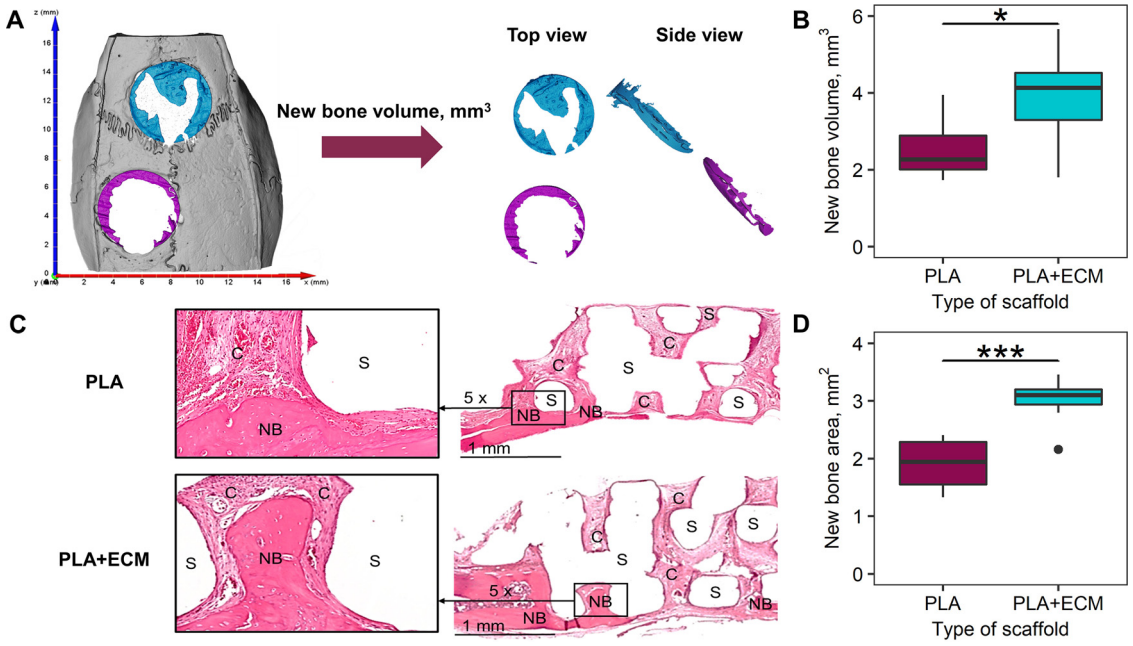

Figure 4. Bone regeneration *in vivo*. (A) Representative processed micro-CT images of volume of newly formed bone (mm^3) in PLA (purple) and PLA+ECM (blue) scaffolds. (B) Box plot representing volume of newly formed bone (mm^3) according to sample groups. (C) Histological section images (hematoxylin and eosin staining). Images on left represent typical findings of samples for both sexes. (D) Box plot representing histology results of the area (mm^2) of newly formed bone according to sample groups. $^*P < 0.05$ and $^{***}P < 0.001$ (indicate significant differences between tested groups). C, connective tissue; NB, new bone; S, scaffold. (Color version of figure is available online.)

decellularization conditions impact ECM structure, and there is also, most importantly, substantial loss of matrisome-associated proteins. Furthermore, these types of bioinks are in limited supply and have huge batch-to-batch variations [48,49].

A promising alternative for decellularized tissues is cell-synthesized ECM [50]. Although different cell types express similar core matrisome components, their produced ECMs trigger distinct biological responses. This phenomenon is determined by both different quantities of the same core components and unique, cell type-specific ECM constituents [27,51,52]. Studies have elucidated the proteomic composition of ECMs derived from BMSCs, ASCs, neonatal dermal fibroblasts and osteoblast/fibroblast co-cultures for bone tissue engineering research [27,28,51,52]. Results have shown that ECM produced by different cell types displays significantly different osteoinductive properties. Although no major differences have been observed between BMSC- and ASC-secreted ECM with regard to cell fate decision [27,52], in Baronceli study [51], BMSCs differentiated to an osteogenic lineage produced more osteoinductive ECM compared with non-differentiated cells. This shows the importance of ECM forming cells to be committed to osteogenic direction.

DPSCs are MSCs with great osteogenic potential [35]. In previous research, the authors showed that DPSCs are capable of differentiating to an osteogenic lineage even without the additional supplements that are usually used in other studies [36,40]. Principally, in the authors' previous *in vivo* research, the scaffolds decorated with DPSC-derived ECM demonstrated the same osteoinductivity potential as the leading bone substitute for regenerative dentistry, Bio-Oss (Geistlisch Pharmaceutical, Wolhusen, Switzerland) [43]. For this reason, in the present study, the same DPSC-formed ECM was characterized and its osteogenic regeneration potential analyzed both *in vitro* and *in vivo*.

After the DPSC-derived ECM proteomic analysis, a total of 403 proteins were detected; however, the majority were not associated with the extracellular region (351). These proteins were intracellular—left over after the decellularization process. The authors chose to ignore them in subsequent analysis since they had no direct impact on cell fate. Although some researchers choose to include all proteins in their analysis [51], this is not the correct procedure, as intracellular proteins (e.g., ribosomal ligands, histones) have no impact outside the cell. In addition, the authors determined 52 extracellular region proteins. Of these, more than 70% were assigned as core matrisome (16) and matrisome-associated (22) proteins. Despite the fact that DPSCs were grown for 7 days on PLA scaffolds without any chemical differentiation inductors, according to the Enrichr database, their secreted ECMs were directly related to biological processes associated with bone/cartilage formation. This again implies the DPSC osteogenic commitment compared with other MSC sources (e.g., BMSCs, ASCs).

Moreover, both GO analysis of protein biological function and the authors' *in vitro* and *in vivo* data confirmed that DPSC-derived ECM improves the osteoinductivity of PLA scaffolds. Cells grown on ECM-decorated samples had higher ALP activity and showed osteogenic differentiation-related gene expression and significantly upregulated ECM mineralization compared with cells on pure PLA samples. Pivotally, scaffolds coated with DPSC-derived ECM greatly improved regeneration of critical-size bone defects: new bone islands separated from the defect edges were observed in only the PLA+ECM group. DPSC-produced ECM composition was rich in proteins, which could have contributed to the observed *in vitro* and *in vivo* results. For example, the expression of *GREM1* is required for healthy skeletal development and homeostasis [53]. LOX is an extracellular amine oxidase whose function is to catalyze the cross-linking reaction of collagen and elastin in the ECM. In this way, LOX facilitates osteogenic ECM stabilization, development, maturation and remodeling [54,55].

Although matrisome components (e.g., ANAXA1, GREM1, SULF1, LOXL2) are the main factors orchestrating cellular response, other chemical/mechanical/topographical effectors are also important [56]. For example, decellularized scaffolds are rich in calcium deposits, which serve as nucleation sites for new hydroxyapatite crystal formation [25] and lead to enhanced ALP expression and activity in cells [69–71]. Therefore, these factors could have influenced the higher

ECM mineralization and ALP activity in DPSCs grown on PLA+ECM scaffolds since the authors have previously shown the formation of mineralized ECM after 7 days of culturing DPSCs on PLA scaffolds [36,40].

Cell adhesion and migration into the scaffold, followed by proliferation, are crucial processes for successful bone regeneration [57]. ECM formed by various cell types (e.g., BMSCs, osteoblasts, osteoblast/fibroblast co-cultures) significantly improves cell–scaffold interaction [22,26,28]. Here the authors also demonstrated that DPSC-derived ECM increases cell adhesion, migration and proliferation. DPSCs were more widespread and had higher proliferation potential on PLA+ECM surfaces. Moreover, DPSC-formed ECM enhanced not only MSC migration but also primary PTEC migration. Furthermore, DPSC-derived ECM improved endogenous cell migration into PLA+ECM scaffolds implanted in rat skull critical-size defects, as evidenced by hematoxylin and eosin staining and micro-CT analysis showing new bone islands that were separate from the defect edges. According to the authors' proteomic data, DPSC-produced ECM contained proteins, including COL1A1, FN1, ANAXA1, LOXL2 and GREM1, whose signal sequences can be recognized by the cell. During cell–ECM protein interaction, various signaling pathways are initiated, which controls cell survival, migration, proliferation and even differentiation [58–65].

Oxygen and nutrient supply is essential for the vitality and function of all tissues. Indeed, ensuring this is one of the main challenges in tissue engineering hindering implementation of larger tissue constructs [66–68]. Thus, the promotion of angiogenesis, which is overlooked in the majority of tissue engineering studies [69–71], is crucial for regeneration of every tissue. Therefore, the authors evaluated DPSC-derived ECM angioinductivity by following primary PTEC migration into the scaffolds and by determining VEGF production by DPSCs grown on ECM-decorated and pure PLA samples. The results showed that ECM drastically improved angioinductive scaffold properties. Proteomic data also confirmed that DPSC-synthesized ECM is rich in proteins (e.g., LTBP2, SULF1, GREM1, epidermal growth factor-like protein 7), which stimulates angiogenesis. For example, the cytokine GREM1 can activate the VEGFR2-Akt-mTORC2 signaling pathway, which is relevant to angiogenesis [72,73]. Epidermal growth factor-like protein 7 can act as a chemoattractant for endothelial cells [74] or, by interfering with the Notch pathway, can regulate sprouting angiogenesis [75]. Therefore, DPSC-secreted ECM increased the angiogenic potential of tested PLA scaffolds and is a promising technique for improving scaffold integration into tissue.

Transplant rejection is a major problem in implantation surgeries. Rejection is caused by an organism's immune response to the transplanted graft [76]. For this reason, after such medical procedures, patients should use immunosuppressive drugs; however, these medications cause many side effects [77]. Tissue engineering solves this problem because it uses autologous cells to regenerate the tissues [28,78]. Nevertheless, degradation byproducts of the natural or synthetic polymers used for scaffold production can lead to acute or chronic inflammation [79–81]. This has often been ignored in other studies and requires more research [71,82,83].

Here the immunomodulation of PLA scaffolds with DPSC-produced ECM was assessed. According to proteomic results, five proteins (ANXA1, ANXA2, C1QB, TIMP2 and PPIA) were associated with biological processes of the immune system. However, as demonstrated by the literature, all five proteins mediate the inflammatory events required for new bone formation. ANXA1, ANXA2 and C1QB regulate neutrophil recruitment to the sites of inflammation [84–86]. The appropriate number of neutrophils is essential for successful bone fracture healing. Neutrophils migrate to the damage site, where they secrete the biologically active molecules (e.g., IL-6, chemokine ligand 2) that are essential for the attraction of progenitor stem cells from adjacent tissues [87,88]. TIMP2 and PPIA are required for bone remodeling and bone tissue homeostasis; however, their exact mechanism of function is entirely unknown [89,90]. DPSC-formed ECM immunoinductivity was further investigated by analyzing DPSC secretomes grown on PLA+ECM scaffolds. The results revealed that most of the molecules in the secretome are associated with activation (e.g., IL-6, CINC family proteins, soluble intercellular adhesion molecule 1, chemokine [C-X-C motif] ligand family proteins, chemokine [C-C motif] ligand 5) or inhibition (IL-1ra) of inflammatory processes [91–96]. They regulate the migration of neutrophils and macrophages [87,88,91,95,96]. Although PLA+ECM constructs can induce pro-inflammatory cytokine expression, they are essential for coordination of damaged tissue regeneration. *In vivo* histology results confirmed these findings. Cell infiltrates were observed in surrounding newly forming bone tissue. Cell infiltrates are usually composed of lymphocytes, macrophages and multi-nucleated giant cells, which are responsible for the degradation of foreign objects and new tissue formation.

Conclusions

DPSC-secreted ECM was investigated for use in applications for artificial bone tissue construction. Results showed that surface decoration with DPSC-formed ECM improved the properties required for successful bone regeneration. The authors identified a unique ECM protein network ornamenting the surface, with a suitable microenvironment that enhanced cell attachment, migration, proliferation, immunomodulation, osteogenesis and angiogenesis. This protein network recruited endogenous stem cells, stimulating the self-healing process in bone defects. Therefore, DPSC-secreted ECM may be a promising tool for decorating various biomaterials for use in bone tissue engineering. Nevertheless, additional studies in which the synergistic effects of ECM with different scaffold formulations are evaluated are needed.

Funding

This work was supported by the L'Oréal Baltic "For Women in Science" fellowship with the support of the Lithuanian National Commission for the United Nations Educational, Scientific and Cultural Organization and the Lithuanian Academy of Sciences, and by Vilnius University Scientific Funds funded project No. MSF-JM-9/2021.

Declaration of Competing Interest

The authors have no commercial, proprietary or financial interest in the products or companies described in this article.

Author Contributions

MA conducted the research, performed the statistical analysis and wrote/revised the paper. MK conducted the cell culture experiments. ES prepared composite materials, designed and 3D printed scaffolds, reviewed manuscript. IR prepared the illustrations. IG conducted in vivo expirements. PB conducted cytokine evaluation study and revised manuscript. AK performed proteomic ECM evaluation. DS performed immunohistochemical analysis. VR designed the research. VB directed the project and contributed to the idea. All authors have approved the final article.

Supplementary materials

Supplementary material associated with this article can be found in the online version at doi:10.1016/j.jcyt.2022.02.002.

References

[1] Ansari M. Bone tissue regeneration: biology, strategies and interface studies. Prog. Biomater. 2019;8:223–37.
[2] Dimitriou R, Jones E, McGonagle D, Giannoudis PV. Bone regeneration: current concepts and future directions. BMC Med 2011;9:66.
[3] De Witte T-M, Fratila-Apachitei LE, Zadpoor AA, Peppas NA. Bone tissue engineering via growth factor delivery: from scaffolds to complex matrices. Regen. Biomater. 2018;5:197–211.
[4] Chen S, Guo Y, Liu R, Wu S, Fang J, Huang B, Li Z, Chen Z, Chen Z. Tuning surface properties of bone biomaterials to manipulate osteoblastic cell adhesion and the signaling pathways for the enhancement of early osseointegration. Colloids Surfaces B Biointerfaces 2018;164:58–69.
[5] Ho-Shui-Ling A, Bolander J, Rustom LE, Johnson AW, Luyten FP, Picart C. Bone regeneration strategies: Engineered scaffolds, bioactive molecules and stem cells current stage and future perspectives. Biomaterials 2018;180:143–62.
[6] Roseti L, Parisi V, Petretta M, Cavallo C, Desando G, Bartolotti I, Grigolo B. Scaffolds for Bone Tissue Engineering: State of the art and new perspectives. Mater. Sci. Eng. C. 2017;78:1246–62.
[7] Laurencin C, Khan Y, El-Amin SF. Bone graft substitutes. Expert Rev. Med. Devices. 2006;3:49–57.
[8] Ghassemi T, Shahroodi A, Ebrahimzadeh MH, Mousavian A, Movaffagh J, Moradi A. Current Concepts in Scaffolding for Bone Tissue Engineering. Arch. Bone Jt. Surg 2018;6:90–9.
[9] Santo VE, Gomes ME, Mano JF, Reis RL. Controlled release strategies for bone, cartilage, and osteochondral engineering-part i: Recapitulation of native tissue healing and variables for the design of delivery systems. Tissue Eng. Part B Rev. 2013;19:308–26.
[10] Gerstenfeld LC, Cullinane DM, Barnes GL, Graves DT, Einhorn TA. Fracture healing as a post-natal developmental process: Molecular, spatial, and temporal aspects of its regulation. J. Cell. Biochem. 2003;88:873–84.
[11] Kaigler D, Wang Z, Horger K, Mooney DJ, Krebsbach PH. VEGF scaffolds enhance angiogenesis and bone regeneration in irradiated osseous defects. J. Bone Miner. Res. 2006;21:735–44.
[12] Lin X, Shanmugasundaram S, Liu Y, Derrien A, Nurminskaya M, Zamora PO. B2A peptide induces chondrogenic differentiation *in vitro* and enhances cartilage repair in rats. J. Orthop. Res. 2012;30:1221–8.
[13] Lindley EM, Guerra FA, Krauser JT, Matos SM, Burger EL, Patel VV. Small peptide (P-15) bone substitute efficacy in a rabbit cancellous bone model. J. Biomed. Mater. Res. B. Appl. Biomater. 2010;94:463–8.
[14] Oh S, Moon KS, Lee SH. Effect of RGD peptide-coated TiO2 nanotubes on the attachment, proliferation, and functionality of bone-related cells. J. Nanomater. 2013;2013:1–11. https://doi.org/10.1155/2013/965864.
[15] Hum J, Boccaccini AR. Collagen as coating material for 45S5 bioactive glass-based scaffolds for bone tissue engineering. Int. J. Mol. Sci. 2018;19(6):1807. https://doi.org/10.3390/ijms19061807.
[16] Mohamadyar-Toupkanlou F, Vasheghani-Farahani E, Hanaee-Ahvaz H, Soleimani M, Dodel M, Havasi P, Ardeshirylajimi A, Taherzadeh ES. Osteogenic Differentiation of MSCs on Fibronectin-Coated and nHA-Modified Scaffolds. ASAIO J 2017;63:684–91.
[17] Ying X, Sun L, Chen X, Xu H, Guo X, Chen H, Hong J, Cheng S, Peng L. Silibinin promotes osteoblast differentiation of human bone marrow stromal cells via bone morphogenetic protein signaling. Eur. J. Pharmacol. 2013;721:225–30.
[18] Gao YH, Yamaguchi M. Suppressive Effect of Genistein on Rat Bone Osteoclasts: Apoptosis Is Induced through Ca2+ Signaling. Biol. Pharm. Bull. 1999;22:805–9.
[19] Zhou Y, Wu Y, Jiang X, Zhang X, Xia L, Lin K, Xu Y. The Effect of Quercetin on the Osteogenesic Differentiation and Angiogenic Factor Expression of Bone Marrow-Derived Mesenchymal Stem Cells. PLoS One 2015;10:e0129605.
[20] Wu Y, Cao L, Xia L, Wu Q, Wang J, Wang X, Xu L, Zhou Y, Xu Y, Jiang X. Evaluation of Osteogenesis and Angiogenesis of Icariin in Local Controlled Release and Systemic Delivery for Calvarial Defect in Ovariectomized Rats. Sci. Rep. 2017;7:5077.
[21] Kutys ML, Doyle AD, Yamada KM. Regulation of cell adhesion and migration by cell-derived matrices. Exp. Cell Res. 2013;319:2434–9.
[22] Kim B, Ventura R, Lee B-T. Functionalization of porous BCP scaffold by generating cell-derived extracellular matrix from rat bone marrow stem cells culture for bone tissue engineering. J. Tissue Eng. Regen. Med. 2018;12:e1256–67.
[23] Kim YS, Majid M, Melchiorri AJ, Mikos AG. Applications of decellularized extracellular matrix in bone and cartilage tissue engineering. Bioeng. Transl. Med. 2019;4:83–95.
[24] Liao J, Guo X, Grande-Allen KJ, Kasper FK, Mikos AG. Bioactive polymer/extracellular matrix scaffolds fabricated with a flow perfusion bioreactor for cartilage tissue engineering. Biomaterials 2010;31:8911–20.
[25] Liao J, Guo X, Nelson D, Kasper FK, Mikos AG. Modulation of osteogenic properties of biodegradable polymer/extracellular matrix scaffolds generated with a flow perfusion bioreactor. Acta Biomater 2010;6:2386–93.
[26] Burgio F, Rimmer N, Pieles U, Buschmann J, Beaufils-Hugot M. Characterization and in ovo vascularization of a 3D-printed hydroxyapatite scaffold with different extracellular matrix coatings under perfusion culture. Biol. Open. 2018;7:bio034488.
[27] Harvestine JN, Orbay H, Chen JY, Sahar DE, Leach JK. Cell-secreted extracellular matrix, independent of cell source, promotes the osteogenic differentiation of human stromal vascular fraction. J. Mater. Chem. B. 2018;6:4104–15.
[28] Li M, Zhang A, Li J, Zhou J, Zheng Y, Zhang C, Xia D, Mao H, Zhao J. Osteoblast/fibroblast coculture derived bioactive ECM with unique matrisome profile facilitates bone regeneration. Bioact. Mater. 2020;5:938–48.
[29] Zhang C, Li M, Zhu J, Luo F, Zhao J. Enhanced bone repair induced by human adipose-derived stem cells on osteogenic extracellular matrix ornamented small intestinal submucosa. Regen. Med. 2017;12:541–52.
[30] Parmaksiz M, Elçin AE, Elçin YM. Decellularized Cell Culture ECMs Act as Cell Differentiation Inducers. Stem Cell Rev. Reports. 2020;16:569–84.
[31] Tamaki Y, Nakahara T, Ishikawa H, Sato S. *In vitro* analysis of mesenchymal stem cells derived from human teeth and bone marrow. Odontology 2013;101:121–32.
[32] Alge DL, Zhou D, Adams LL, Wyss BK, Shadday MD, Woods EJ, Chu TMG, Goebel WS. Donor-matched comparison of dental pulp stem cells and bone marrow-derived mesenchymal stem cells in a rat model. J. Tissue Eng. Regen. Med. 2010;4:73–81.
[33] Logovskaya L V, Bukharova TB, Volkov A V, Vikhrova EB, Makhnach O V, Goldshtein D V. Induction of Osteogenic Differentiation of Multipotent Mesenchymal Stromal Cells from Human Adipose Tissue. Bulletin of Experimental Biology and Medicine 2013;155(1):145–50. https://doi.org/10.1007/s10517-013-2100-x.
[34] Mori G, Brunetti G, Oranger A, Carbone C, Ballini A, Muzio LLo, Colucci S, Mori C, Grassi FR, Grano M. Dental pulp stem cells: osteogenic differentiation and gene expression. Ann. N. Y. Acad. Sci. 2011;1237:47–52.
[35] Pierdomenico L, Bonsi L, Calvitti M, Rondelli D, Arpinati M, Chirumbolo G, Becchetti E, Marchionni C, Alviano F, Fossati V, Staffolani N, Franchina M, Grossi A, Bagnara GP. Multipotent mesenchymal stem cells with immunosuppressive activity can be easily isolated from dental pulp. Transplantation 2005;80:836–42.
[36] Alksne M, Kalvaityte M, Simoliunas E, Rinkunaite I, Gendviliene I, Locs J, Rutkunas V, Bukelskiene V. *In vitro* comparison of 3D printed polylactic acid/hydroxyapatite and polylactic acid/bioglass composite scaffolds: Insights into materials for bone regeneration. J. Mech. Behav. Biomed. Mater. 2020;104:103641.
[37] Wiśniewski JR, Zougman A, Nagaraj N, Mann M. Universal sample preparation method for proteome analysis. Nat. Methods. 2009;6:359–62.
[38] Naba A, Clauser KR, Ding H, Whittaker CA, Carr SA, Hynes RO. The extracellular matrix: Tools and insights for the "omics" era. Matrix Biol 2016;49:10–24.
[39] Šimoliūnas E, Kantakevičius P, Kalvaitytė M, Bagdzevičiūtė L, Alksnė M, Baltriukienė D. DNA-DAPI Interaction-Based Method for Cell Proliferation Rate Evaluation in 3D Structures. Curr. Issues Mol. Biol. 2021;43:251–63.
[40] Alksne M, Simoliunas E, Kalvaityte M, Skliutas E, Rinkunaite I, Gendviliene I, et al. The effect of larger than cell diameter polylactic acid surface patterns on osteogenic differentiation of rat dental pulp stem cells. J. Biomed. Mater. Res. - Part A. 2019;107:174–86. https://doi.org/10.1002/jbm.a.36547.
[41] Livak KJ, Schmittgen TD. Analysis of relative gene expression data using real-time quantitative PCR and the 2-ΔΔCT method. Methods 2001;25:402–8.
[42] Faul F, Erdfelder E, Lang AG, Buchner A. G*Power 3: a flexible statistical power analysis program for the social, behavioral, and biomedical sciences. Behav. Res. Methods, Psychonomic Society Inc. 2007;39(2):175–91.
[43] Gendviliene I, Simoliunas E, Alksne M, Dibart S, Jasiuniene E, Cicenas V, Jacobs R, Bukelskiene V, Rutkunas V. Effect of extracellular matrix and dental pulp stem cells on bone regeneration with 3D printed PLA/HA composite scaffolds. Eur. Cells Mater. 2021;41:204–15.
[44] Hynes RO, Naba A. Overview of the matrisome-An inventory of extracellular matrix constituents and functions. Cold Spring Harb. Perspect. Biol. 2012;4(1):a004903. https://doi.org/10.1101/cshperspect.a004903.
[45] Frantz C, Stewart KM, Weaver VM. The extracellular matrix at a glance. J. Cell Sci. 2010;123:4195–200.
[46] Pati F, Jang J, Ha D-H, Won Kim S, Rhie J-W, Shim J-H, Kim D-H, Cho D-W. Printing three-dimensional tissue analogues with decellularized extracellular matrix bioink. Nat. Commun. 2014;5:3935.
[47] Sobreiro-Almeida R, Quinteira R, Neves NM. Renal Regeneration: The Role of Extracellular Matrix and Current ECM-Based Tissue Engineered Strategies. Adv. Healthc. Mater. 2021;10:2100160.
[48] Crapo PM, Gilbert TW, Badylak SF. An overview of tissue and whole organ decellularization processes. Biomaterials 2011;32:3233–43.
[49] Hillebrandt KH, Everwien H, Haep N, Keshi E, Pratschke J, Sauer IM. Strategies based on organ decellularization and recellularization. Transpl. Int. 2019;32:571–85.
[50] Thibault RA, Mikos AG, Kasper FK. Protein and mineral composition of osteogenic extracellular matrix constructs generated with a flow perfusion bioreactor. Biomacromolecules 2011;12:4204–12.
[51] Baroncelli M, van der Eerden BC, Kan Y-Y, Alves RD, Demmers JA, van de Peppel J, van Leeuwen JP. Comparative proteomic profiling of human osteoblast-derived extracellular matrices identifies proteins involved in mesenchymal stromal cell osteogenic differentiation and mineralization. J. Cell. Physiol. 2018;233:387–95.
[52] Ragelle H, Naba A, Larson BL, Zhou F, Prijić M, Whittaker CA, Del Rosario A, Langer R, Hynes RO, Anderson DG. Comprehensive proteomic characterization of stem cell-derived extracellular matrices. Biomaterials 2017;128:147–59.
[53] Canalis E, Parker K, Zanotti S. Gremlin1 is required for skeletal development and postnatal skeletal homeostasis. J. Cell. Physiol. 2012;227:269–77.
[54] Cai L, Xiong X, Kong X, Xie J. The Role of the Lysyl Oxidases in Tissue Repair and Remodeling: A Concise Review. Tissue Eng. Regen. Med. 2017;14:15–30.
[55] Gartland A, Erler JT, Cox TR. The role of lysyl oxidase, the extracellular matrix and the pre-metastatic niche in bone metastasis. J. Bone Oncol. 2016;5:100–3.
[56] Alksne M, Simoliunas E, Kalvaityte M, Skliutas E, Rinkunaite I, Gendviliene I, Baltriukiene D, Rutkunas V, Bukelskiene V. The effect of larger than cell diameter polylactic acid surface patterns on osteogenic differentiation of rat dental pulp stem cells. J. Biomed. Mater. Res. Part A. 2019;107:174–86.
[57] Polo-Corrales L, Latorre-Esteves M, Ramirez-Vick JE. Scaffold design for bone regeneration. J. Nanosci. Nanotechnol. 2014;14:15–56.

[58] Holle AW, McIntyre AJ, Kehe J, Wijesekara P, Young JL, Vincent LG, Engler AJ. High content image analysis of focal adhesion-dependent mechanosensitive stem cell differentiation. Integr. Biol. (United Kingdom) 2016;8:1049–58.
[59] Kumar A, Nune KC, Misra RDK. Biological functionality of extracellular matrix-ornamented three-dimensional printed hydroxyapatite scaffolds. J. Biomed. Mater. Res. Part A. 2016;104:1343–51.
[60] Provenzano PP, Keely PJ. Mechanical signaling through the cytoskeleton regulates cell proliferation by coordinated focal adhesion and Rho GTPase signaling. J. Cell Sci. 2011;124:1195–205.
[61] Pin AL, Houle F, Fournier P, Guillonneau M, Paquet ÉR, Simard MJ, Royal I, Huot J. Annexin-1-mediated endothelial cell migration and angiogenesis are regulated by vascular endothelial growth factor (VEGF)-induced inhibition of miR-196a expression. J. Biol. Chem. 2012;287:30541–51.
[62] Bizzarro V, Belvedere R, Dal Piaz F, Parente L, Petrella A. Annexin A1 Induces Skeletal Muscle Cell Migration Acting through Formyl Peptide Receptors. PLoS One 2012;7:e48246.
[63] de Jong OG, van der Waals LM, Kools FRW, Verhaar MC, van Balkom BWM. Lysyl oxidase-like 2 is a regulator of angiogenesis through modulation of endothelial-to-mesenchymal transition. J. Cell. Physiol. 2019;234:10260–9.
[64] Huang H, Huang H, Li Y, Liu M, Shi Y, Chi Y, Zhang T. Gremlin induces cell proliferation and extra cellular matrix accumulation in mouse mesangial cells exposed to high glucose via the ERK1/2 pathway. BMC Nephrol 2013;14:33.
[65] Te Hsiao C, Cheng HW, Huang CM, Li HR, Ou MH, Huang JR, Khoo KH, Yu HW, Chen YQ, Wang YK, Chiou A, Kuo JC. Fibronectin in cell adhesion and migration via N-glycosylation. Oncotarget 2017;8:70653–68.
[66] Maté-Sánchez de Val JE, Mazón P, Calvo-Guirado JL, Ruiz RAD, Ramírez Fernández MP, Negri B, Abboud M, De Aza PN. Comparison of three hydroxyapatite/β-tricalcium phosphate/collagen ceramic scaffolds: an *in vivo* study. J. Biomed. Mater. Res. Part A. 2014;102:1037–46.
[67] Hankenson KD, Dishowitz M, Gray C, Schenker M. Angiogenesis in bone regeneration. Injury 2011;42:556–61.
[68] Calabrese G, Giuffrida R, Forte S, Fabbi C, Figallo E, Salvatorelli L, Memeo L, Parenti R, Gulisano M, Gulino R. Human adipose-derived mesenchymal stem cells seeded into a collagen-hydroxyapatite scaffold promote bone augmentation after implantation in the mouse. Sci. Rep. 2017;7:1–11.
[69] Xie Y, Sun W, Yan F, Liu H, Deng Z, Cai L. Icariin-loaded porous scaffolds for bone regeneration through the regulation of the coupling process of osteogenesis and osteoclastic activity. Int. J. Nanomedicine. 2019;14:6019–33.
[70] Wu Z, Meng Z, Wu Q, Zeng D, Guo Z, Yao J, et al. Biomimetic and osteogenic 3D silk fibroin composite scaffolds with nano MgO and mineralized hydroxyapatite for bone regeneration. J Tissue Eng 2020;11:2041731420967791. https://doi.org/10.1177/2041731420967791.
[71] Diez-Escudero A, Harlin H, Isaksson P, Persson C. Porous polylactic acid scaffolds for bone regeneration: a study of additively manufactured triply periodic minimal surfaces and their osteogenic potential. J Tissue Eng 2020;11:2041731420956541. https://doi.org/10.1177/2041731420956541.
[72] Liu Y, Chen Z, Cheng H, Chen J, Qian J. Gremlin promotes retinal pigmentation epithelial (RPE) cellproliferation, migration and VEGF production via activating VEGFR2-Akt-mTORC2 signaling. Oncotarget 2017;8:979–87.
[73] Stabile H, Mitola S, Moroni E, Belleri M, Nicoli S, Coltrini D, Peri F, Pessi A, Orsatti L, Talamo F, Castronovo V, Waltregny D, Cotelli F, Ribatti D, Presta M. Bone morphogenic protein antagonist Drm/gremlin is a novel proangiogenic factor. Blood 2007;109:1834–40.
[74] Nichol D, Stuhlmann H. EGFL7: a unique angiogenic signaling factor in vascular development and disease. Blood 2012;119:1345.
[75] Usuba R, Pauty J, Soncin F, Matsunaga YT. EGFL7 regulates sprouting angiogenesis and endothelial integrity in a human blood vessel model. Biomaterials 2019;197:305–16.
[76] J. Charles A Janeway, P. Travers, M. Walport, M.J. Shlomchik, Responses to alloantigens and transplant rejection, (2001). https://www.ncbi.nlm.nih.gov/books/NBK10757/.
[77] Tönshoff B. Immunosuppressants in Organ Transplantation. Handb. Exp. Pharmacol. 2020;261:441–69.
[78] Edri R, Gal I, Noor N, Harel T, Fleischer S, Adadi N, Green O, Shabat D, Heller L, Shapira A, Gat-Viks I, Peer D, Dvir T. Personalized Hydrogels for Engineering Diverse Fully Autologous Tissue Implants. Adv. Mater. 2019;31:1803895.
[79] Yang F, Niu X, Gu X, Xu C, Wang W, Fan Y. Biodegradable Magnesium-Incorporated Poly(l-lactic acid) Microspheres for Manipulation of Drug Release and Alleviation of Inflammatory Response. ACS Appl. Mater. Interfaces. 2019;11:23546–57.
[80] Li D, Sun H, Jiang L, Zhang K, Liu W, Zhu Y, Fangteng J, Shi C, Zhao L, Sun H, Yang B. Enhanced biocompatibility of PLGA nanofibers with gelatin/nano-hydroxyapatite bone biomimetics incorporation. ACS Appl. Mater. Interfaces. 2014;6:9402–10.
[81] Ma S, Feng X, Liu F, Wang B, Zhang H, Niu X. The pro-inflammatory response of macrophages regulated by acid degradation products of poly(lactide-co-glycolide) nanoparticles. Eng. Life Sci 2021;21(10):709–20. https://doi.org/10.1002/elsc.202100040.
[82] Velioglu ZB, Pulat D, Demirbakan B, Ozcan B, Bayrak E, Erisken C. 3D-printed poly (lactic acid) scaffolds for trabecular bone repair and regeneration: scaffold and native bone characterization. Connect Tissue Res 2018;60(3):274–82. https://doi.org/10.1080/03008207.2018.1499732.
[83] Zhang B, Wang L, Song P, Pei X, Sun H, Wu L, Zhou C, Wang K, Fan Y, Zhang X. 3D printed bone tissue regenerative PLA/HA scaffolds with comprehensive performance optimizations. Mater. Des. 2021;201:109490.
[84] Swisher JFA, Khatri U, Feldman GM. Annexin A2 is a soluble mediator of macrophage activation. J. Leukoc. Biol. 2007;82:1174–84.
[85] Sugimoto MA, Vago JP, Teixeira MM, Sousa LP. Annexin A1 and the Resolution of Inflammation: Modulation of Neutrophil Recruitment, Apoptosis, and Clearance. J. Immunol. Res. 2016;2016:1–13. https://doi.org/10.1155/2016/8239258.
[86] Leigh LEA, Ghebrehiwet B, Perera TPS, Bird IN, Strong P, Kishore U, Reid KBM, Eggleton P. C1q-mediated chemotaxis by human neutrophils: involvement of gClqR and G-protein signalling mechanisms. Biochem. J. 1998;330:247–54.
[87] Claes L, Recknagel S, Ignatius A. Fracture healing under healthy and inflammatory conditions. Nat. Rev. Rheumatol. 2012;8:133–43.
[88] Schlundt C, El Khassawna T, Serra A, Dienelt A, Wendler S, Schell H, van Rooijen N, Radbruch A, Lucius R, Hartmann S, Duda GN, Schmidt-Bleek K. Macrophages in bone fracture healing: Their essential role in endochondral ossification. Bone 2018;106:78–89. https://doi.org/10.1016/j.bone.2015.10.019.
[89] Guo M, James AW, Kwak JH, Shen J, Yokoyama KK, Ting K, et al. Cyclophilin A (CypA) Plays Dual Roles in Regulation of Bone Anabolism and Resorption. Sci. Rep. 2016;6:1–10.
[90] Liang HPH, Xu J, Xue M, Jackson C. Matrix metalloproteinases in bone development and pathology: current knowledge and potential clinical utility. Met. Med. 2016;3:93–102.
[91] Lorenzetti BB, Veiga FH, Canetti CA, Poole S, Cunha FQ, Ferreira SH. CINC-1 mediates the sympathetic component of inflammatory mechanical hypersensitivitiy in rats. Eur. Cytokine Netw. 2003;13:456–61.
[92] Tanaka T, Narazaki M, Kishimoto T. IL-6 in inflammation, immunity, and disease. Cold Spring Harb. Perspect. Biol. 2014;6:16295–6.
[93] Aldinucci D, Colombatti A. The inflammatory chemokine CCL5 and cancer progression. Mediators Inflamm 2014;2014:1–12. https://doi.org/10.1155/2014/292376.
[94] Perrier S, Darakhshan F, Hajduch E. IL-1 receptor antagonist in metabolic diseases: Dr Jekyll or Mr Hyde? FEBS Lett 2006;580:6289–94.
[95] Sawant KV, Poluri KM, Dutta AK, Sepuru KM, Troshkina A, Garofalo RP, Rajarathnam K. Chemokine CXCL1 mediated neutrophil recruitment: role of glycosaminoglycan interactions. Sci. Rep. 2016;6:1–8.
[96] Ichikawa A, Kuba K, Morita M, Chida S, Tezuka H, Hara H, Sasaki T, Ohteki T, Ranieri VM, Dos Santos CC, Kawaoka Y, Akira S, Luster AD, Lu B, Penninger JM, Uhlig S, Slutsky AS, Imai Y. CXCL10-CXCR3 enhances the development of neutrophil-mediated fulminant lung injury of viral and nonviral origin. Am. J. Respir. Crit. Care Med. 2013;187:65–77.